

Spiral Breakup in Excitable Tissue due to Lateral Instability

A. F. M. Marée and A. V. Panfilov

Department of Theoretical Biology, University of Utrecht, Padualaan 8, 3584 CH Utrecht, The Netherlands
(Received 27 March 1996)

In a simple two-component model of excitable tissue a spiral wave is found to break up into a large number of small spirals. More specifically, we used a modified FitzHugh-Nagumo model. Spiral breakup is found to occur when the recovery variable diffuses at a high rate. The breakup is caused by lateral instability of the wave front. We analyzed this instability using quasi-one-dimensional computations and found that it could be connected to a negative eikonal-curvature relation for the parameter values at which spiral breakup occurs. [S0031-9007(97)02568-4]

PACS numbers: 87.10.+e, 05.45.+b, 82.20.Wt, 82.40.Bj

Recent studies have demonstrated that spiral waves in excitable media can be generated by a phenomenon called spiral breakup [1–8]. This phenomenon was discussed recently in connection with the mechanisms of cardiac fibrillation [9,10]; spiral breakup has also been found in experiments with the Belousov-Zhabotinskii (BZ) reaction [11–15]. The mechanism has been discussed in several papers [5–7]. It was found to occur in models that show spatiotemporal instabilities of wave trains in one-dimensional (1D) excitable media. The mechanism of this 1D instability is believed to be associated with the restitution properties of excitable tissue [16,17].

However, experimental data of Markus and Stavridis suggest another possible cause of spiral breakup [12,13]. In their experiments the wave fronts develop a curly shape before they break down into chaos. This curly shape is similar to the shape that is expected to occur when the wave front is laterally unstable [18]. The mechanism of this instability is associated with a negative slope of the so-called eikonal-curvature relationship. In this paper we report on the spiral breakup occurring in a two-component FitzHugh-Nagumo (FHN) model due to lateral instability.

The lateral instability of a wave front is related to a change in the slope of the eikonal-curvature relationship. This relationship expresses the normal velocity V of a wave as a function of its curvature k . Convex and concave waves are defined by $k > 0$ and $k < 0$, respectively. It is possible to derive the following relationship for waves with a small curvature: $V = V_0 - Dk$, where V_0 is the velocity of a planar wave, and D a constant usually referred to as the effective diffusion coefficient (D_{eff}) [19]. Wave instabilities occur if D_{eff} is negative [18]. Therefore we studied the dependence of the velocity of the front on its curvature in a modified FHN model [6] in which we incorporated diffusion for both the recovery and the activator variable. We computed the value of D_{eff} from this dependency, and by using a genetic algorithm we were able to find parameter settings for which $D_{\text{eff}} < 0$. To determine the eikonal relationship, and to calculate D_{eff} , we used fast quasi-1D computations of the eikonal equation with constant curvature of the wave [19]. In this equation, curvature and direction of motion are pre-

defined. The diffusion term is given by $\Delta = \frac{\partial^2}{\partial \xi^2} + k \frac{\partial}{\partial \xi}$, where k is the curvature and ξ the direction perpendicular to the wave.

We used the following model for an excitable medium, based on piecewise linear ‘‘Pushchino kinetics’’:

$$\begin{aligned} \frac{\partial e}{\partial t} &= \Delta e - f(e) - g, \\ \frac{\partial g}{\partial t} &= D_g \Delta g + \varepsilon(e, g)(ke - g), \end{aligned} \quad (1)$$

with $f(e) = C_1 e$ when $e < e_1$; $f(e) = -C_2 e + a$ when $e_1 \leq e \leq e_2$; $f(e) = C_3(e - 1)$ when $e > e_2$, and $\varepsilon(e, g) = \varepsilon_1$ when $e < e_2$; $\varepsilon(e, g) = \varepsilon_2$ when $e > e_2$, and $\varepsilon(e, g) = \varepsilon_3$ when $e < e_1$ and $g < g_1$. To make the function $f(e)$ continuous, $e_1 = a/(C_1 + C_2)$ and $e_2 = (a + C_3)/(C_2 + C_3)$. Using genetic algorithms, we found the following basic parameter values at which we studied spiral breakup: $C_1 = 43.3$, $C_2 = 6.5$, $C_3 = 18.3$, $a = 0.64$, $k = 9.1$, $g_1 = 1.95$, $\varepsilon_1^{-1} = 49.4$, $\varepsilon_2^{-1} = 4.4$, and $\varepsilon_3^{-1} = 2.8$. The shape of the function $f(e)$ specifies the fast processes. The dynamics of the recovery variable g in the model are determined by the function $\varepsilon(e, g)$. In $\varepsilon(e, g)$ the parameter ε_1^{-1} specifies the recovery time constant for relatively large values of g and intermediate values of e . This region corresponds approximately to the wave front, wave back, and to the absolute refractory period. Similarly, ε_2^{-1} and ε_3^{-1} specify the recovery time constant for large values of e , and for small values of e and g , respectively. These regions correspond approximately to the excited period, and to the relative refractory period, respectively. The dynamics of g at the wave front and wave back are slow, but during the excited and the relative refractory period the dynamics are faster. The only difference between this model and the previous model [6] is that this model incorporates diffusion of both the activator and the recovery variable.

For numerical computations we used the explicit Euler method with Neumann boundary conditions. To determine the velocity of waves with a fixed curvature, a wave was initiated in the linear grid, and its velocity was measured after it had become constant. This procedure was

repeated for different curvatures. To initiate the first spiral in a rectangular grid we used initial data corresponding to a broken wave, the break being located in the middle of the excitable tissue.

We found that spiral breakup occurred spontaneously in the excitable media at high values of D_g . Figure 1 shows the evolution of a spatial pattern in a medium with $D_g = 2.55$. The spatial pattern starts to form as soon as one spiral wave has developed. This spiral makes several rotations [Fig. 1(a)]. The spiral wave becomes perforated [Fig. 1(b)], then becomes more and more perforated, and breaks into several interacting spiral waves of different sizes [Fig. 1(c)]. Finally, when there is a high density of small spirals, the pattern becomes relatively stable [Fig. 1(d)]. These spirals are randomly distributed in space, but their centers remain in approximately fixed positions.

The process by which the spirals in our case were formed is shown in Fig. 2. The initial plane wave front becomes unstable. In particular, part of the wave front becomes retarded, the delay increases, and finally the wave breaks up and an excited spot is formed. This spot interacts with the following wave and creates two wave breaks, which develop into two spiral waves.

The breakup that occurred in our model was not due to discrete properties of our medium. We did computations

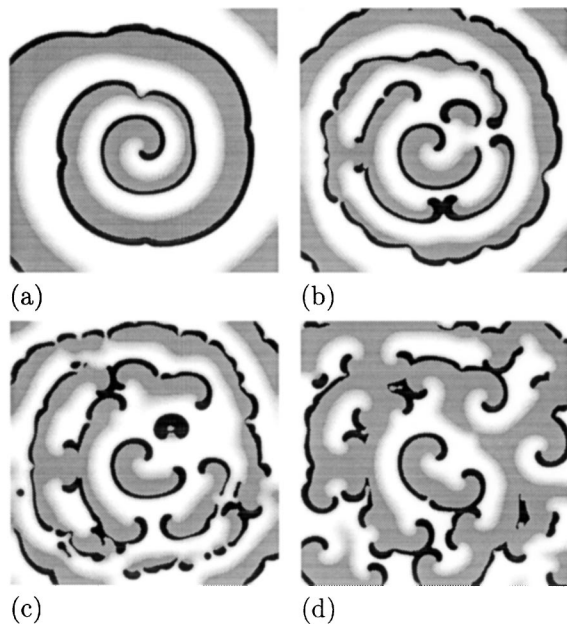


FIG. 1. The spiral breakup in model (1). The snapshots are at time (a) $t = 144$, (b) $t = 208$, (c) $t = 252$, and (d) $t = 608$. Numerical integration was done with space step $h_s = 0.15$, and time step $h_t = 0.0011$, on a grid of 1333×1333 elements. Black represents the excited state of the tissue ($e > 0.6$), dark gray shows the region where $g > 1.95$ (close to the absolute refractory state), and intermediate shading from gray to white shows different levels of g , $0.3 < g < 1.95$ (estimate of the relative refractory period).

for a wide variety of space steps ($0.05 \leq h_s \leq 0.85$). We studied the stability of spiral breakup at various spatial and time integration steps, and found that the patterns were similar for different degrees of calculation precision, but the value of the parameter D_g at which spiral breakup occurs increased as the calculation precision increased. We found that at $h_s < 0.2$ the shift saturated.

The mechanism of such breaks is due to the lateral instability of wave fronts. Figure 3 shows the relation between velocity V of a wave and its curvature k at the same parameter values at which we find breakup. We see that, for $k < 0.3$, velocity increases with increasing curvature, i.e., the wave front here is unstable because of the lateral instability. For $k > 0.3$, velocity decreases with increasing curvature and wave fronts are stable again. The spiral cores are stable because they have the highest curvature.

The observation that, for small curvatures, velocity increases with curvature can be understood from a cross section through the wave. The insets of Fig. 3 show the values of e and g in such a cross section, for a straight and a convex wave, respectively. The velocity of a straight wave is restrained by g ahead of the wave front. On the other hand, in the case of a convex wave, the influx of g into the region before the wave front is smaller, which leads to relatively low values of g and faster front propagation. This phenomenon is expected to be fairly general for excitable media with a high diffusion of the recovery variable [18].

By applying regression analysis to the slope around $k = 0$ we calculated the D_{eff} [Fig. 4(a)]. At $D_g \approx 2.12$, $D_{\text{eff}} = 0$. Spiral breakup is found when $D_{\text{eff}} < -1.2$, i.e., at $2.5 < D_g < 2.6$. At higher values of D_g , propagationless patterns are found. We observed several types of propagationless patterns with static and oscillatory behavior, comparable with and occurring in the same succession as the patterns described by Ohta, Mimura, and Kobayashi [20].

We studied the dependence of the lateral instability and spiral breakup on the parameters of the excitable medium. We computed two values of D_g for different parameter settings. The first value (D_{g1}) is the value of

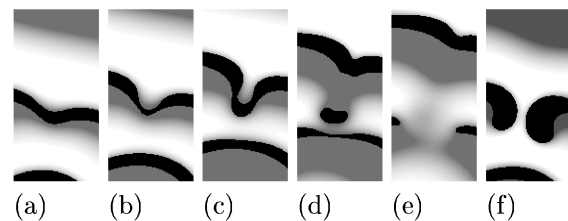


FIG. 2. Development of spiral breakup due to lateral instability. Enlargement of Fig. 1 region where first breakup occurred, measuring 172×352 elements. The snapshots are at time (a) $t = 140$, (b) $t = 144$, (c) $t = 148$, (d) $t = 152$, (e) $t = 156$, and (f) $t = 164$. Gray-scale coding is the same as in Fig. 1.

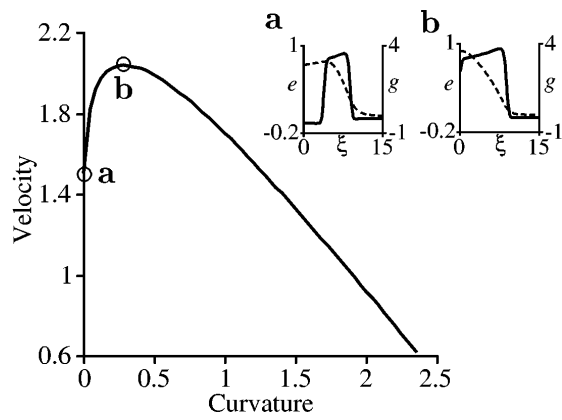


FIG. 3. The relation between curvature and velocity of a wave. The insets show the values of e (solid lines) and g (dashed lines) in cross sections through the wave; (a) for a straight wave, and (b) for a convex wave, with curvature $k = 0.28$. Computations were done on a linear grid of 1000 elements. Numerical integration was the same as in Fig. 1.

D_g at which $D_{\text{eff}} = 0$, and the second value (D_{g2}) is the value of D_g at which propagationless patterns are found. The procedure was the following: We changed the value of one parameter and, by varying the value of D_g , we found the values D_{g1} and D_{g2} . The results are shown in Fig. 4(b). For example, for “basic values” of parameters and numerical precision as given in the figure caption, we get propagationless patterns at $D_g \geq 1.98$ and lateral instability ($D_{\text{eff}} < 0$) at $D_g \geq 1.68$ [large open circle in Fig. 4(b)]. We changed nine parameters, and found that all nine lines of $D_{g1}(D_{g2})$ are located in a small region. The differences in D_{g1} are less than 10% for $D_{g2} < 3$ and less than 20% for $D_{g2} > 3$. Hence we can conclude that lateral instability is a general property of this model. We can also conclude that a good prediction of the occurrence

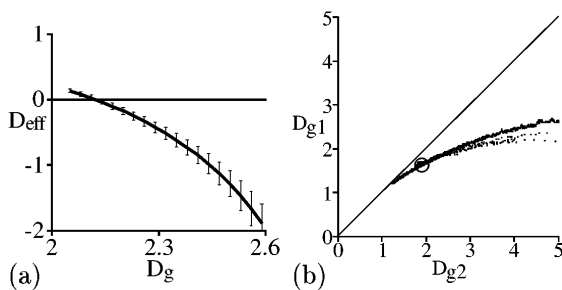


FIG. 4. (a) D_{eff} , calculated with a regression analysis for $k \approx 0$. For $2.15 < D_g < 2.6$, D_{eff} has a negative sign. For $D_g > 2.6$, only stationary patterns are found. Numerical integration was the same as in Fig. 3. (b) Lowest value of D_g at which propagationless patterns are found (D_{g2}) against the value of D_g at which $D_{\text{eff}} = 0$ (D_{g1}) for 4346 different parameter settings. Every time one parameter was changed, the other parameters were kept at the basic values. The large open circle shows the position for basic values. Numerical integration was done with space step $h_s = 0.45$, and time step $h_t = 0.010$, on a linear grid of 444 elements.

of lateral instability can be made by using the value of D_{g2} : For $D_{g2} > 1.2$ we observed lateral instabilities.

Low values of D_{g2} , at which there was no lateral instability, were found for media with low excitability. Low excitability can be caused by a high threshold (parameter a high), by a rapid increase of g during the excited period (parameter k high, or parameters ϵ_1^{-1} , ϵ_2^{-1} , or C_3 low), or by entering the refractory period at low values of g (parameter C_2 low). For example, for “basic” parameter values and numerical precision as given in Fig. 4(b), $D_{g2} = 1.98$, while $D_{g2} = 1.2$ when a is changed to 0.98, or k to 17.3, or ϵ_1^{-1} to 2.7, or ϵ_2^{-1} to 1.9, or C_3 to 5.1, or C_2 to 5.1.

At higher values of D_{g2} , the interval of values of D_g for which we have lateral instability increases. However, lateral instability does not necessarily lead to spiral breakup for several reasons. First, a large refractory period prevents spiral breakup, even when the wave front is laterally unstable [Fig. 5(a)]. This is found when ϵ_3^{-1} is high or g_1 is low. In our case, if we increased ϵ_3^{-1} to 10, or decreased g_1 to 0.9, spiral breakup disappeared. It explains why spiral breakup by lateral instability is difficult to find in models with only one, slow, time constant for the recovery variable. Second, a large size of the excited region, i.e., where $e > 0.6$, prevents spiral breakup [Fig. 5(b)]. In these cases the instability is not

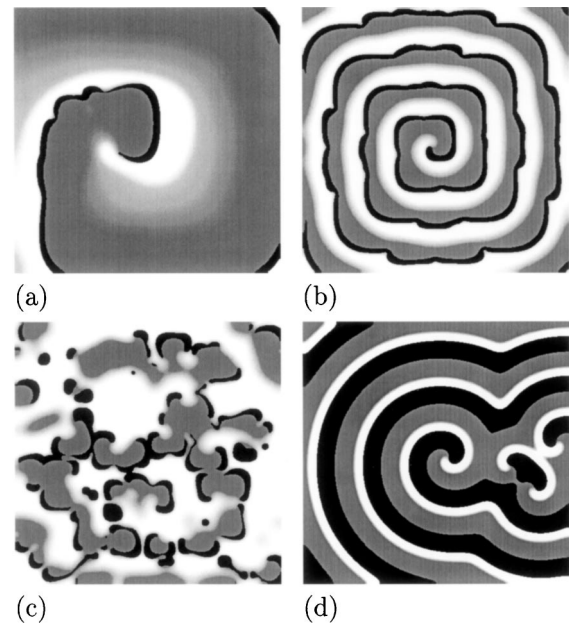


FIG. 5. (a) Spiral breakup prevented by large refractory period; $g_1 = 0.9$, $D_g = 1.93$, and $D_{\text{eff}} = -1.5$. (b) Spiral breakup prevented by a large size of the excited region; $\epsilon_3^{-1} = 2.0$, $D_g = 2.08$, and $D_{\text{eff}} = -1.4$. (c) Chaotic pattern of appearing and disappearing spirals; $\epsilon_1^{-1} = 1000.0$, $D_g = 2.45$, and $D_{\text{eff}} = -4.4$. (d) Stable spirals found in the autocycling regime; $C_1 = 1.8$, $D_g = 2.6$, and $D_{\text{eff}} = -7.5$. Numerical integration was the same as in Fig. 4(b), on a grid of 444×444 elements. Gray-scale coding is the same as in Fig. 1.

strong enough to form new spirals. This is also the case partially because the large excited region is accompanied by a large refractory period. A large excited region is found when the threshold is low (parameter a low), when the increase of g during the excited period is slow (parameter k low, or parameters ε_2^{-1} or C_3 high), when the system enters the refractory period at very high values of g (parameter C_2 high), or when there is a fast decrease of g behind the excited region (parameter ε_3^{-1} low, or parameter g_1 high). For example, if we increased ε_2^{-1} to 7.1, C_3 to 90.0, or C_2 to 7.9, or decreased a to 0.34, k to 6.5, or ε_3^{-1} to 2.0, breakup disappeared. Third, if ε_1^{-1} or C_1 are high, the refractory period is large, but spiral breakup is found to occur in the core of the spiral. This eventually leads to a chaotic pattern of appearing and disappearing spirals [Fig. 5(c)]. The mechanism is a mixture of the spatiotemporal instabilities, as described earlier [5–7], and the lateral instability, as described in this paper. We found this behavior when we increased C_1 to 250, or ε_1^{-1} to 100. Fourth, when C_1 is decreased to 0.7, the spatially uniform system (1) passes a point of fold bifurcation for limit cycles. This causes the system to autocycle after an initial stimulation. However, even before the bifurcation point ($C_1 < 2.3$) autocycling can be found in the spatial model. Such behavior was recently described in [21]. The autocycling pushes aside all irregularities as caused by the lateral instability [Fig. 5(d), $C_1 = 1.8$]. Even considering the above points, we still find breakup by lateral instability in a fairly large region of the parameter space.

The wave patterns obtained in our computations are similar to those obtained in the experiments performed by Marcus [11–13]. The mechanisms of the instabilities are also similar. In the light-sensitive BZ reaction the slope of the eikonal-curvature dependence was found to be both positive and humped [12], just as in our computations. However, it is not clear which mechanisms generate the positive slope in the BZ reaction. In our model the positive slope occurs because of the large diffusion coefficient of the inhibitor. In the light-sensitive BZ reaction the diffusions of chemical species are of the same order of magnitude. However, in the case of the BZ reaction, an increase in the concentration inhibitor Br^- is determined by its diffusion coefficient multiplied by the rate constant of its autocatalysis. It is known that light enhances the production of Br^- , and it may be this enhanced increase in the Br^- concentration which leads to the curly wave fronts and spiral breakups [12].

The mechanism of instability that causes the spiral breakup described in this paper is fundamentally different from the 1D instability which is responsible for the earlier observations of spiral breakup [5–7]. First, it is a pure two-dimensional mechanism, and it has no counterpart in 1D systems. Second, not only wave trains, but also solitary waves show this instability.

Although lateral instabilities of wave fronts have not been described earlier in models for excitable media, they have been found in bistable systems [22,23]. Horváth *et al.* found an unstable wave front but no spiral breakup [22]. Hagberg and Meron showed that lateral instability made turbulence possible through Ising-Bloch front bifurcations [23]. An analytical study of other types of spatial instabilities of wave trains was reported in [24].

We expect the phenomenon of spiral breakup by lateral instability to be not uncommon in excitable media and that it is probably easy to find comparable behavior in other models of excitable media with nonfixed time scales for the recovery variable.

We are grateful to Professor P. Hogeweg for valuable discussions and help in this research. We wish to thank S.M. McNab for linguistic advice. A.F.M. Marée is supported by the Priority Program Nonlinear Systems of the Netherlands Organization for Scientific Research.

-
- [1] A. Winfree, *J. Theor. Biol.* **138**, 353 (1989).
 - [2] A. Panfilov and A. Holden, *Phys. Lett. A* **151**, 23 (1990).
 - [3] M. Gerhardt, H. Schuster, and J. Tyson, *Science* **247**, 1563 (1990).
 - [4] M. Courtemanche and A. Winfree, *Int. J. Bifurcation Chaos Appl. Sci. Eng.* **1**, 431 (1991).
 - [5] H. Ito and L. Glass, *Phys. Rev. Lett.* **66**, 671 (1991).
 - [6] A. Panfilov and P. Hogeweg, *Phys. Lett. A* **176**, 295 (1993).
 - [7] A. Karma, *Phys. Rev. Lett.* **71**, 1103 (1993).
 - [8] M. Bär and M. Eiswirth, *Phys. Rev. E* **48**, R1635 (1993).
 - [9] A. Winfree, *Science* **266**, 1003 (1994).
 - [10] A. Panfilov and P. Hogeweg, *Science* **270**, 1223 (1995); response by A. T. Winfree, *ibid.* **270**, 1224 (1995).
 - [11] M. Marcus, G. Kloss, and I. Kusch, *Nature (London)* **371**, 402 (1994).
 - [12] M. Marcus and K. Stavridis, *Int. J. Bifurcation Chaos Appl. Sci. Eng.* **4**, 1233 (1994).
 - [13] M. Marcus and K. Stavridis, *Philos. Trans. R. Soc. London A* **347**, 601 (1994).
 - [14] Z. Nagy-Ungvarai and S. Müller, *Int. J. Bifurcation Chaos Appl. Sci. Eng.* **4**, 1257 (1994).
 - [15] Q. Ouyang and J.-M. Flesselles, *Nature (London)* **379**, 143 (1996).
 - [16] M. Courtemanche, L. Glass, and J. Keener, *Phys. Rev. Lett.* **70**, 2182 (1993).
 - [17] A. Karma, *Chaos* **4**, 461 (1994).
 - [18] Y. Kuramoto, *Prog. Theor. Phys.* **63**, 1885 (1980).
 - [19] J. Keener, *J. Math. Biol.* **29**, 629 (1991).
 - [20] T. Ohta, M. Mimura, and R. Kobayashi, *Physica (Amsterdam)* **34D**, 115 (1989).
 - [21] I. Tsyganov, M. Tsyganov, A. Medvinsky, and G. Ivanitsky, *Dokl. Akad. Nauk* **346**, 825 (1996).
 - [22] D. Horváth, V. Petrov, S. Scott, and K. Showalter, *J. Chem. Phys.* **98**, 6332 (1993).
 - [23] A. Hagberg and E. Meron, *Phys. Rev. Lett.* **72**, 2494 (1994).
 - [24] D. Kessler and H. Levine, *Phys. Rev. A* **41**, 5418 (1990).